THE ASTROPHYSICAL JOURNAL, 399:611–620, 1992 November 10


# FAR-ULTRAVIOLET OBSERVATIONS OF THE CRAB NEBULA USING THE HOPKINS ULTRAVIOLET TELESCOPE

WILLIAM P. BLAIR,[1] KNOX S. LONG,[2] OLAF VANCURA,[1] CHARLES W. BOWERS,[1] SARAH CONGER,[1]
ARTHUR F. DAVIDSEN,[1] GERARD A. KRISS,[1] AND RICHARD B. C. HENRY[3]

*Received 1992 February 19; accepted 1992 May 18*

## ABSTRACT

We have observed the far-ultraviolet spectrum (912–1860 Å) of the central portion of the Crab Nebula supernova remnant using the Hopkins Ultraviolet Telescope aboard the *Astro-1* space shuttle mission in 1990 December. The synchrotron power-law continuum, greatly attenuated by interstellar absorption, can be seen extending down to $\sim$1000 Å before being lost in the noise. The C IV $\lambda$1549 emission line shows two resolved components representing the front and back sides of the shell expanding at roughly $\pm$1100 km s$^{-1}$. This agrees well with the velocity distribution of optical [O III] emission at the same location in the Crab. The He II $\lambda$1640 emission line, however, shows only a blueshifted component corresponding to the near side of the shell. These are the first observations to demonstrate that relative UV line intensity variations are present in the Crab Nebula. No other emission lines intrinsic to the Crab Nebula's filaments have been detected over the HUT wavelength range. We compare the HUT observation to optical emission-line imagery and to archival *IUE* observations. This comparison indicates that a distributed emission component, consisting of either a number of individually faint filaments or a diffuse component, produces the bulk of the emission seen by HUT. A grid of photoionization models for the Crab Nebula filaments is calculated to infer the range of ionization conditions and/or abundances that are needed to account for the observed UV line ratios and limits. Assuming that the diffuse redshifted and blueshifted emission seen with HUT arises in material of similar ionization parameter, the differing UV line ratios observed for these components probably indicates varying carbon and/or He abundances are present in the observed material.

*Subject headings:* ISM: individual (Crab Nebula) — supernova remnants — ultraviolet: interstellar

## 1. INTRODUCTION

The Crab Nebula (SN 1054) provides one of the nearest and best examples of a young supernova remnant (SNR), and as such it has provided many clues about the supernova phenomenon. The presence of a pulsar in the Crab Nebula, along with its attendant optical/X-ray synchrotron nebula, provides the strongest evidence for the creation of pulsars in some supernova explosions. Yet in many respects the Crab Nebula is peculiar among young SNRs. The velocity of the expanding nebular filaments ($\pm$1500 km s$^{-1}$) is much lower than seen in some young remnants such as Cas A (age $\sim$310 yr, $V_{exp} \simeq \pm$8500 km s$^{-1}$; Fesen, Becker, & Goodrich 1988) and SN 1006 (age $\sim$985 yr, $V_{exp} \simeq \pm$3000 km s$^{-1}$; Smith et al. 1991), and the optical filaments are photoionized by the diffuse synchrotron continuum (energized by the pulsar) instead of shock-excited as in most young remnants. Thus, the Crab Nebula has been called everything from "prototypical" to "atypical" by various investigators over the years. An excellent observational review is provided by Davidson & Fesen (1985), and the conference proceedings edited by Kafatos & Henry (1985) also include a number of significant results on the Crab Nebula and other similar SNRs.

Much of the Crab's uniqueness is thought to be the result of the progenitor's mass. Many arguments, including the presence of a neutron star, estimates of the mass and composition of the nebula, and models of stellar evolution and supernovae all indicate a mass range of 8–12 $M_\odot$ for the progenitor of the Crab. Current estimates of the nebular mass plus neutron star are in the range 2.5–4 $M_\odot$ (MacAlpine & Uomoto 1991); assuming this to represent the "core mass" at the time of the supernova, stellar evolution models (see Nomoto 1984) imply progenitor masses $\sim$4 times this core mass value. Some stellar evolution calculations indicate that stars with initial masses less than 8 $M_\odot$ cannot produce neutron stars (see Nomoto et al. 1982; Weidemann & Koester 1983). On the other hand, evolved stars more massive than $\sim$12 $M_\odot$ are expected to produce ejecta rich in oxygen and its burning products (see Woosley & Weaver 1982); such abundances are not observed in the Crab (Henry 1986; MacAlpine et al. 1989).

The mass range near 10 $M_\odot$ is interesting from the standpoint of stellar evolution calculations because stars above and below this mass are predicted to evolve quite differently from one another in their cores (Nomoto et al. 1982) and require different explosion mechanisms (Nomoto 1984). These effects yield varying abundances in the ejecta, especially for He, C, O, and N. Through careful measurement of these abundances in the ejecta one would hope to refine the mass of the Crab precursor even further.

Fesen & Kirshner (1982) have demonstrated the extent of the variations in relative optical line intensities from various emission knots. Unfortunately, it is difficult to disentangle abundance variations from variations in physical conditions (i.e., ionization effects, density variations) in the Crab filaments. These "filaments" themselves are not simple structures; they most likely have dense neutral "cores" surrounded by higher ionization "envelopes." Modeling such structures is not

[1] Department of Physics and Astronomy, The Johns Hopkins University, Charles & 34th Streets, Baltimore, MD 21218
[2] Space Telescope Science Institute, 3700 San Martin Drive, Baltimore, MD, 21218
[3] Department of Physics and Astronomy, University of Oklahoma, Norman, OK 73019.

simple, as evidenced by the differing results from the two groups who have seriously attempted to do so (Henry & MacAlpine 1982; Pequignot & Dennefeld 1982). Various authors have attempted abundance analyses using simplifying assumptions (Miller 1978; Davidson 1978, 1979). In the case of He/H, Uomoto & MacAlpine (1987) assume that all of the $He^+$ and $H^+$ emission comes from recombinations to determine that most of the nebular gas (typically 75% by mass) is He. MacAlpine et al. (1989) suggest that a central "torus" of filaments may be as much as 95% He by mass. There now seems little doubt that He/H is high and spatially variable in the Crab Nebula, but quantifying this result remains a difficult task.

For other elements, one would like to observe several ionization stages to determine accurate abundances. This is impossible with optical/near IR data alone for some critical elements such as carbon. Carbon only has [C I] $\lambda\lambda$9823,9850 and a very weak permitted C II line at 4267 Å (see Davidson 1979). Dennefeld & Andrillat (1981) found variations in the relative line intensities of [C I] and [S III] in the near-IR spectra of Crab filaments. However, neutral species such as [C I] are particularly difficult to use for abundance studies because the conditions in the regions producing these emissions are poorly constrained by observations. Hence, ultraviolet spectra are especially valuable for this element.

Although the Crab Nebula is bright in the optical, it is a difficult target in the ultraviolet because of substantial interstellar reddening along the line of sight. Results from ANS (Wu 1981) and various optical line ratios (Miller 1973; Fesen & Kirshner 1982) are consistent with $E(B-V) = 0.5$ mag, but concerns about collisional enhancement of the Balmer lines blending of different velocity components in the H$\alpha$ – [N II] region, and mixing of material within spectrograph apertures has prevented an accurate determination of $E(B-V)$. Distance measurements based on velocity and proper motion studies of the filaments place the Crab at $\sim$2.0 kpc and nearly 200 pc out of the Galactic plane ($b^{II} = -5.^{\circ}9$). Even though some dust has been identified in the Crab (Fesen & Blair 1990; Hester et al. 1990), the bulk of the reddening is thought to be interstellar.

The only previous ultraviolet spectroscopic observations of the Crab are those of Davidson et al. (1982) using *IUE*. These observations concentrated on a bright region of filaments $\sim 1'$ SW of the pulsar (their position I; Miller's [1978] optical position 2), although an *IUE* position on bright continuum emission adjacent to the pulsar (position II) was also observed. The SWP spectra of *IUE* position I (hereafter *IUE*-P1) showed emission lines of C IV $\lambda$1549, He II $\lambda$1640, and [C III] $\lambda$1908[4] with roughly equal intensity, but no lines of O or N. Davidson et al. (1982) derive rough abundances for *IUE*-P1 using ions of similar ionization and find $N(C)/N(O) \simeq 1$ and $N(N)/N(C) \leq 1$. Both *IUE* positions showed a substantial UV synchrotron continuum well-fitted with a relation near $\lambda I_\lambda \propto \lambda^{-0.5}$ (after correction for extinction). However, the Crab is very nearly at the limit of *IUE*'s sensitivity, and observations of $\sim$6 other positions within the nebula have yielded blank exposures or very marginal results.

In this paper, we report far-ultraviolet spectra of the Crab Nebula obtained with the Hopkins Ultraviolet Telescope, which flew aboard the space shuttle *Columbia* as part of the *Astro-1 Observatory* in 1990 December (see Blair & Gull 1990 for a description of the *Observatory*). We also report a reanalysis of the *IUE* data for the Crab Nebula since they bear on the interpretation of our new spectra. We use optical CCD/interference filter images to investigate possible spatial variations of the emission within the spectrograph aperture. In § 2 we discuss the observations and data reduction, with our interpretation and results given in § 3. A brief summary is given in § 4.

## 2. OBSERVATIONS AND REDUCTIONS

### 2.1. *HUT Spectroscopy*

New far-ultraviolet spectroscopic observations were carried out with the Hopkins Ultraviolet Telescope (HUT) as part of the *Astro-1* space shuttle mission (STS-35) in 1990 December. HUT consists of an f/2–0.9 m mirror that feeds a prime focus spectrograph with a microchannel-plate intensifier and photon-counting detector. In first order the spectrograph covers the region from 830 to 1860 Å at 0.51 Å pixel$^{-1}$ with a nominal resolution of $\sim$3 Å. Details of the spectrograph and telescope performance on orbit can be found in Davidsen et al. (1992).

The Crab Nebula observation discussed here was made on 1990 December 6 at 6:08 UT. A $17'' \times 116''$ aperture was placed on the nebula as shown in Figures 1*a–d* (Plates 23–24), with the long dimension of the aperture at a position angle of 45°. (The images in Fig. 1 will be described in the next section.) The projected size of the aperture at the assumed distance of 2.0 kpc is 0.17 pc × 1.14 pc; there is no intrinsic spatial resolution within this large aperture. With the large spectrograph aperture used here and the extended nature of the target, the spectral resolution was degraded to $\sim$6 Å. Blind positioning relative to nearby pre-planned guide stars was used to center the aperture at $\alpha(1950) = 05^h31^m28^s.7$, $\delta(1950) = 21^{\circ}58'40''.9$. The total integration was slightly over 2000 s. The last $\sim$300 s of the observation were in orbital day and are severely contaminated by airglow emissions; also, pointing difficulties affect the first 500 s of data. Hence, these data have been excluded from this analysis. The primary mirror of the telescope was moved several times during the integration to test the focus of the TV guide camera, but pointing error signals for the guide stars, which come from the TV guider, indicate that pointing remained nominal during these operations. We have inspected various subsections of the data for consistency and variations in airglow contamination. The Crab was within a few degrees of the anti-Sun direction at the time of the observation, but faint airglow lines were still present and variable well before the orbital night-into-day terminator crossing. We have settled on a 1206 s portion of the data from orbital night as the best compromise between signal and minimal airglow contamination and use these data for the analysis which follows.

The reductions of these data included dark count subtraction (using separate dark frames taken for this purpose), a minor correction for detector pulse persistence, subtraction of

[4] The feature seen in *IUE* low-dispersion spectra near wavelength 1908 Å in spectra of many objects such as SNRs, planetary nebulae, and active galaxies has long been recognized as a doublet of $C^{+2}$ at 1907 and 1909 Å. In most tabulations of observed or modeled line intensities, this feature is usually ascribed to C III] (i.e., an intercombination transition). However, as pointed out in Osterbrock (1989), the shorter wavelength line is actually a forbidden transition. The ratio of the two components of this doublet is sensitive to density, with the forbidden line stronger in low-density plasmas (e.g., SNRs) and the intercombination line dominating at higher densities (e.g., active galaxies). While both lines should be present but unresolved in the Crab Nebula spectra, we choose to list the line as [C III] since this component should be stronger.

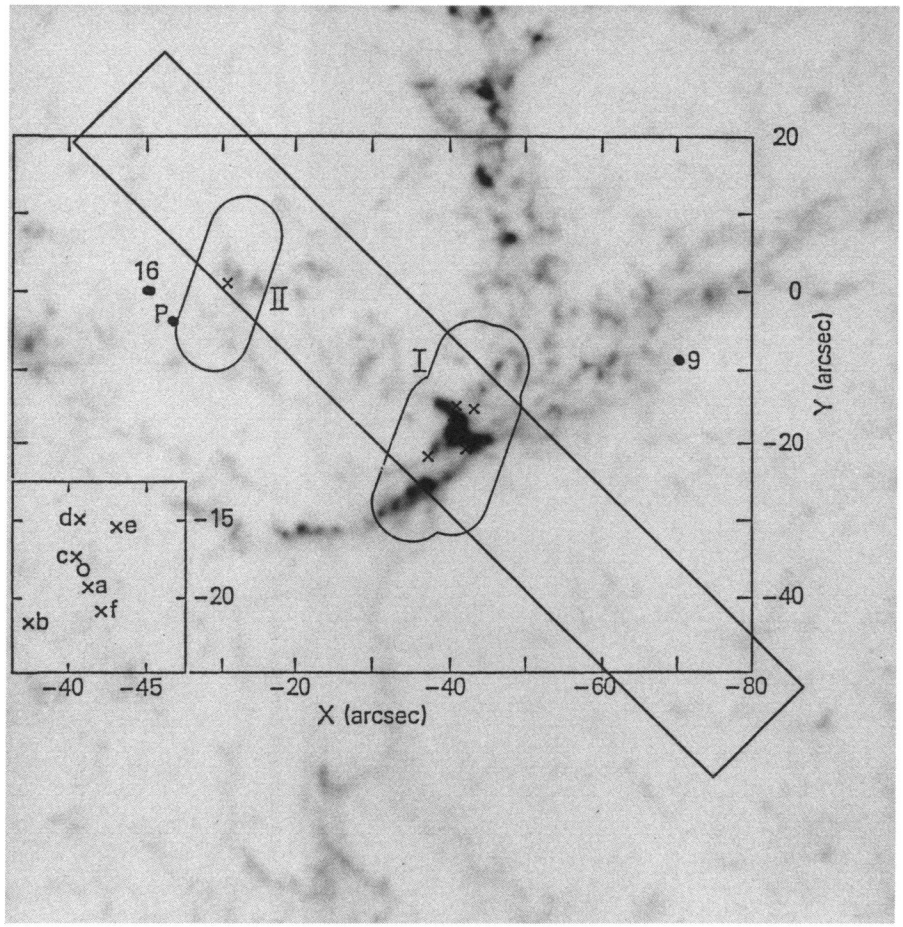


FIG. 1*a*

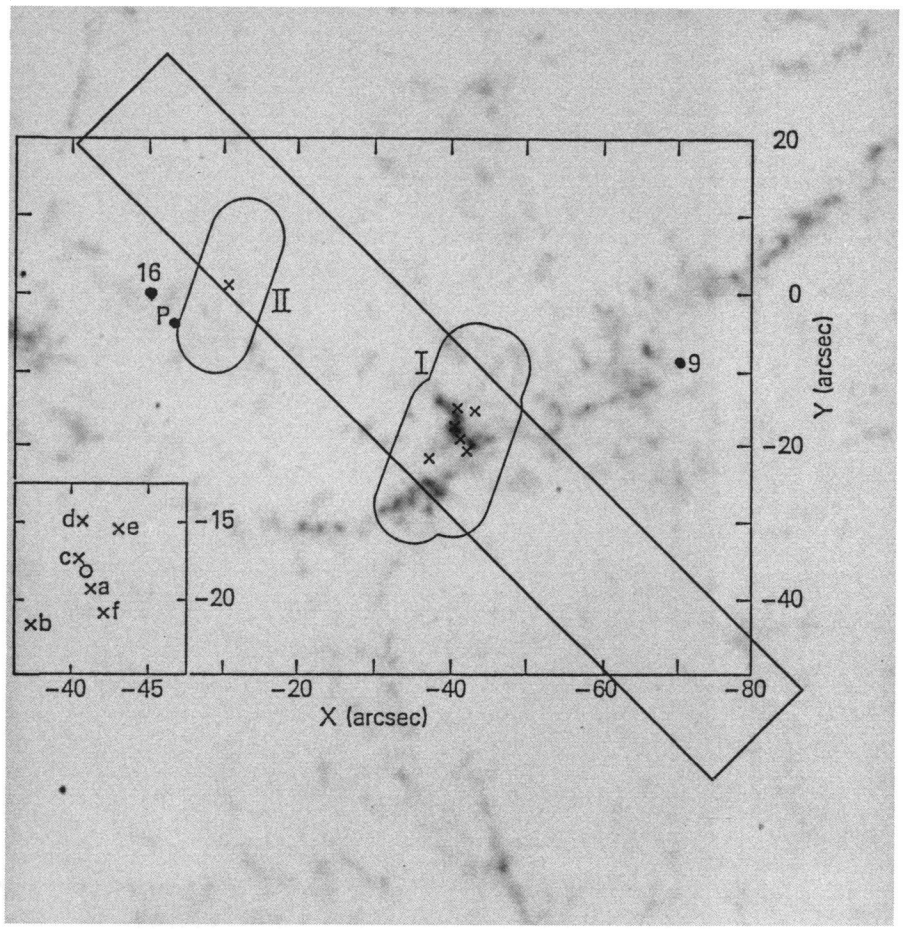


FIG. 1*b*

FIG. 1.—(*a*) Hα, (*b*) [O I] λ6300, (*c*) [O III] λ5007, and (*d*) 6100 Å continuum CCD images of the central portion of the Crab Nebula, obtained at the prime focus of the 4 m Mayall telescope at Kitt Peak National Observatory. North is up, and east is to the left. The location of the HUT 17″ × 116″ aperture is shown to scale as are the *IUE* aperture positions from Davidson et al. (1982). The positions of the pulsar ("P") and several stars in the field are also indicated.

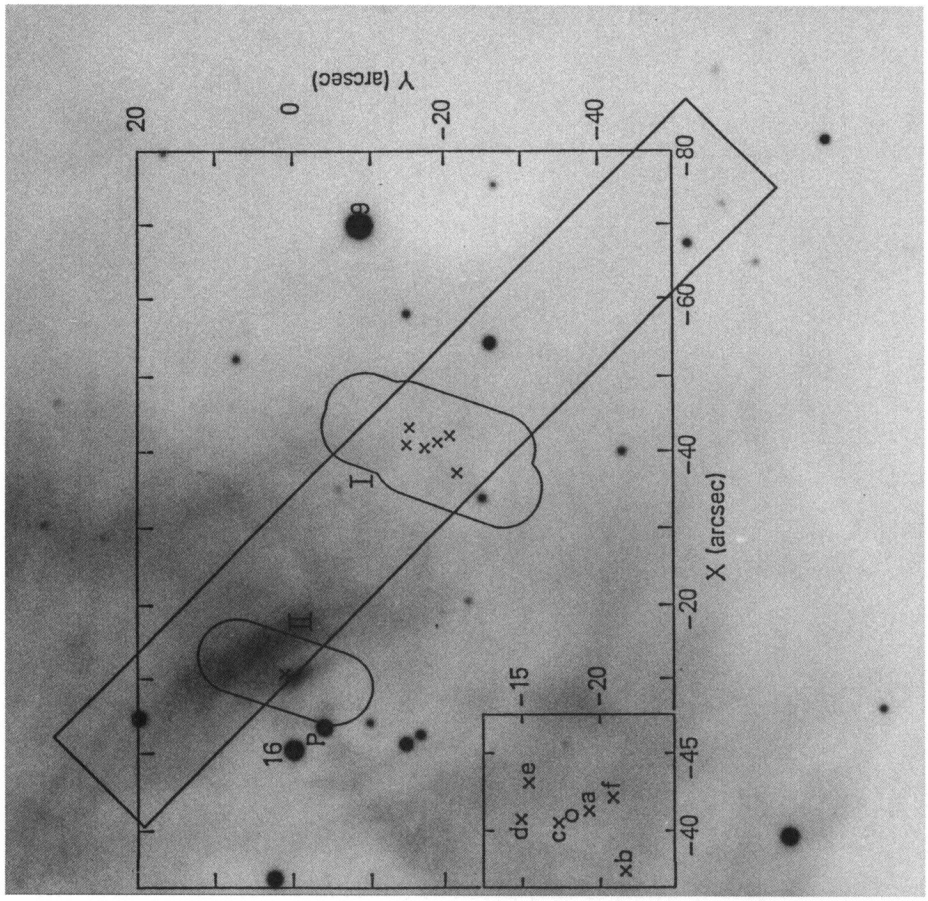


FIG. 1d

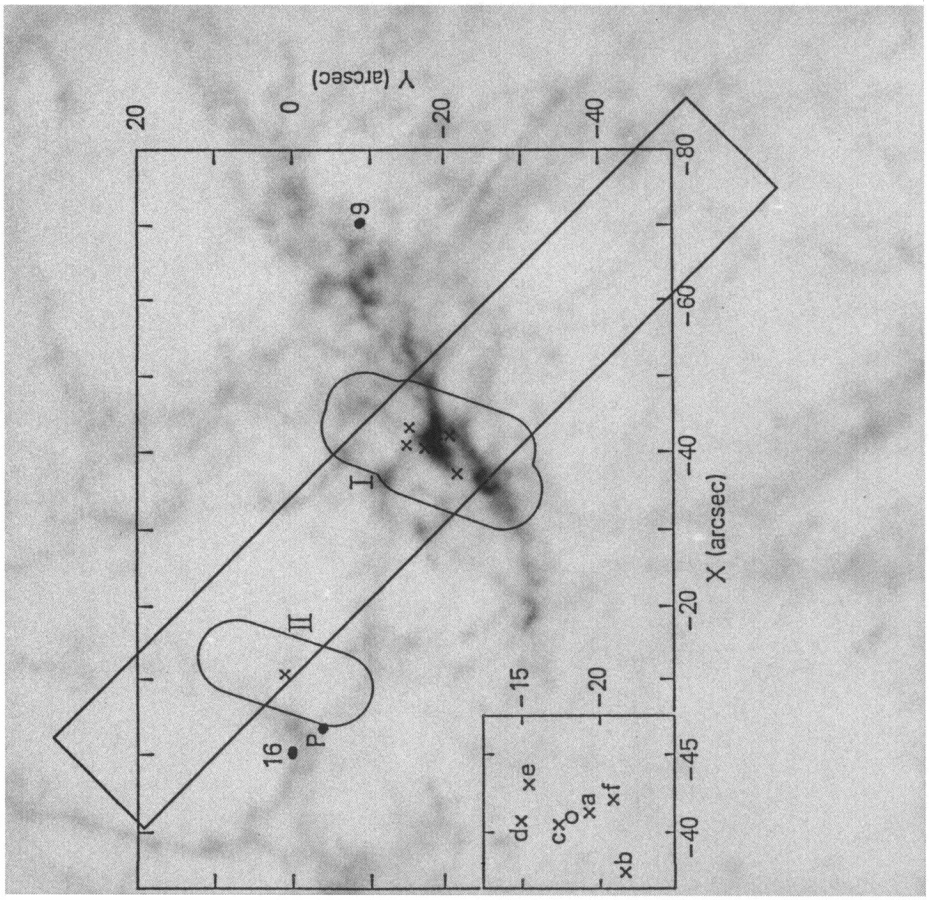


FIG. 1c

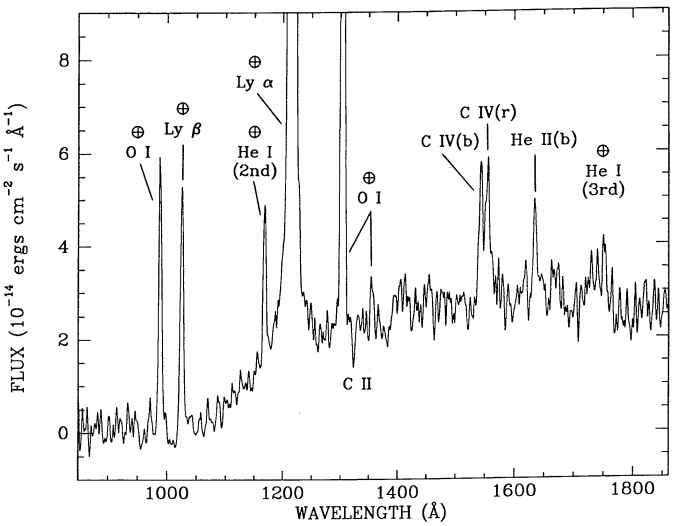


FIG. 2.—The FUV spectrum of the Crab Nebula after conversion to fluxes using in-flight calibration data from the white dwarf G191-B2B. The data have been smoothed with a Gaussian filter of FWHM 5 pixels (~2.5 Å). The only lines intrinsic to the Crab Nebula are from C IV and He II; the remainder of the lines are due to airglow emission. (No correction for airglow contamination has been made in this spectrum, although scattering has been removed.) The intrinsic continuum from the Crab Nebula is too heavily attenuated by interstellar absorption below ~1000 Å to be detected.

scattered light (due mostly to geocoronal Lyα through the large aperture) and conversion to fluxes and wavelengths. Our flux calibration is based on observations of the white dwarf star G191-B2B compared with model stellar atmospheres as discussed by Davidsen et al. (1992). The wavelength scale was very stable, judging from the positions of airglow lines with known wavelengths and in general is good to within ±0.5 Å. Figure 2 shows the reduced flux-calibrated spectrum after smoothing with a Gaussian filter of FWHM 5 pixels.

Observed and reddening-corrected emission line fluxes and upper limits are shown in Table 1. These measurements were made using a $\chi^2$ minimization program called "specfit," which is described in more detail below. The reddening correction has been made using the extinction curve from Seaton (1979) as extended to the Lyman limit by Longo et al. (1989). Significant variations in UV extinction curves along various lines of sight are known (Mathis 1990 and references therein) and the application of the mean galactic curve has obvious but unavoidable hazards. Wu (1981) has shown some evidence for peculiar extinction in the direction toward the Crab using ANS data, but these were broad-band photometric measurements. We assume the standard galactic curve in what follows and search for any evidence of deviations.

The only emission lines clearly detected over our wavelength range are C IV λ1549, which shows two resolved components, and He II λ1640, which shows only one component. (An interstellar absorption line of C II λ1335 is also present at a significant level.) The He II emission line corresponds in velocity to the shorter wavelength component of C IV, both of which are blueshifted by ~1100 km s$^{-1}$ with respect to their rest wavelengths. The other component of C IV is redshifted by ~1000 km s$^{-1}$ and is somewhat broader, perhaps showing some evidence for blended subcomponents. Table 1 also shows upper limits for various other lines, including lines of C, N, O, and and He II λ1640 component that would correspond to the redshifted C IV component. Weak Lyγ airglow emission at 972 Å in conjunction with the large reddening makes placing a significant upper limit on C III λ977 difficult (especially a blueshifted component). The general excess of emission in the 1725–1755 Å region is not seen in other HUT spectra, and it is tempting to ascribe it at least partially to N III] λλ1730, 1750. However, the implied velocity broadening is too large, and the strongest peak (at 1752 Å) is due to geocoronal He I λ584 seen from the third order of the HUT grating. (The second-order feature can be seen in Fig. 2 at 1168 Å.) A similar but weaker excess appears near 1400 Å, which could be marginally detected O IV] emission. These line strengths and limits will be discussed further in § 3.1.

### 2.2. *Optical CCD/Interference Filter Images*

The HUT spectra have no intrinsic spatial resolution within the 17″ × 116″ region sampled by the aperture. However, we

TABLE 1

OBSERVED AND EXTINCTION-CORRECTED[a] HUT AND *IUE* EMISSION-LINE DATA FOR THE CRAB NEBULA

| | | | HUT | | *IUE*-P1 Average | | *IUE*-P1A | | *IUE*-P1B | | *IUE*-P1C | |
|---|---|---|---|---|---|---|---|---|---|---|---|---|
| Ion | λ(lab) | λ(obs)[b] | F(λ) | I(λ) | F(λ) | I(λ) | F(λ) | I(λ) | F(λ) | I(λ) | F(λ) | I(λ) |
| C III | 977 | ... | < 5 | < 110 | ... | ... | ... | ... | ... | ... | ... | ... |
| O VI | 1035 | ... | < 5 | < 50 | ... | ... | ... | ... | ... | ... | ... | ... |
| He II | 1085 | ... | < 10 | < 60 | ... | ... | ... | ... | ... | ... | ... | ... |
| N V | 1240 | (1238.9) | < 14 | < 31 | < 14 | < 31 | < 25 | < 55 | < 5 | < 11 | < 8 | < 18 |
| C II | 1335 | (1331.5) | < 17 | < 25 | < 16 | < 24 | < 22 | < 33 | < 16 | < 24 | < 21 | < 32 |
| Si IV, O IV] | 1400 | ... | < 23 | < 29 | < 25 | < 31 | < 33 | < 41 | < 20 | < 25 | < 25 | < 31 |
| N IV] | 1486 | ... | < 19 | < 21 | < 19 | < 21 | < 30 | < 33 | < 30 | < 33 | < 46 | < 50 |
| C IVb | 1549 | 1543.4 (1545.1) | 100 | 100 | 100 | 100 | 100 | 100 | 100 | 100 | 100 | 100 |
| C IVr | 1549 | 1554.2 | 100 | 100 | < 20 | < 20 | < 25 | < 25 | < 21 | < 21 | < 20 | < 20 |
| He IIb | 1640.5 | 1634.6 (1638.4) | 63 | 61 | 81 | 75 | 142 | 132 | 84 | 78 | 110 | 102 |
| He IIr | 1640.5 | 1645.6 | < 15 | < 13 | < 10 | < 9 | < 10 | < 9 | < 10 | < 9 | < 10 | < 9 |
| O III] | 1663 | ... | < 20 | < 18 | < 18 | < 17 | < 29 | < 27 | < 20 | < 18 | < 21 | < 19 |
| N III] | 1748 | ... | < 25 | < 23 | < 20 | < 18 | < 16 | < 15 | < 21 | < 19 | < 20 | < 18 |
| Si III] | 1885 | ... | ... | ... | < 5 | < 5 | < 16 | < 16 | < 10 | < 10 | < 10 | < 10 |
| [C III] | 1908 | (1904.4) | ... | ... | 86 | 93 | 133 | 144 | 105 | 113 | 150 | 162 |
| F(1550), I(1550) | | | 3.5E-13 | 1.4E-11 | 1.3E-13 | 5.3E-12 | 3.6E-14 | 1.6E-12 | 5.4E-14 | 2.2E-12 | 5.2E-14 | 2.1E-12 |

[a] Reddening correction assumes $E(B-V) = 0.50$ and the extinction curve of Longo et al. 1989.
[b] Wavelengths in parentheses are from *IUE* data; otherwise from HUT data.

TABLE 2

KPNO 4 METER PFCCD/INTERFERENCE FILTER IMAGES OF THE CRAB NEBULA

| Date (1987) | Filter | λ(central) (Å) | Δλ (FWHM) (Å) | ΔV (FWHM) (km s$^{-1}$) | Integration (s) | *IUE*/HUT Counts Ratio[a] |
|---|---|---|---|---|---|---|
| Nov 11..... | [S II] | 6732 | 50 | 2230 | 300 | 0.57 |
| | Hα | 6565 | 30 | 1370 | 300 | 0.45 |
| | [O I] | 6320 | 200 | 9500 | 500 | 0.50 |
| Nov 12..... | He I | 5900 | 71 | 3625 | 1000 | 1.0 |
| | [O III] | 5025 | 50 | 3000 | 300 | 0.35 |
| | 6100 | 6100 | 150 | ... | 500 | 0.075 |
| | 8100 | 8100 | 400 | ... | 300 | 0.075 |
| | [C I] | 9835 | 250 | 7620 | 1200 | 0.47 |
| | [S III] | 9100 | 250 | 8420 | 600 | 0.24:[b] |

[a] Relative number of counts in regions of each image corresponding to the *IUE*-P1 aperture and the HUT aperture.

[b] Affected by relatively poor background subtraction.

can obtain some information about what filaments may be contributing significantly by projecting the HUT aperture onto optical emission-line images of the Crab Nebula. We obtained CCD/interference filter images in several optical emission lines and continuum bands in 1987 November using the KPNO 4 m Mayall telescope at the prime focus. A TI 800 × 800 pixel CCD (spatial scale 0.″30 pixel$^{-1}$) was used with narrow interference filters to obtain the exposures summarized in Table 2. The effective seeing for these images ranges from 0.″9–1.″2 FWHM.

These data have been reduced by subtracting bias and normalizing with averages of a number of dome flat-field exposures taken through each filter each night. Even though the emission-line interference filters are fairly narrow, significant continuum emission is passed along with the emission lines. The continuum exposures were obtained in spectral regions uncontaminated by emission lines. Comparison of these continuum frames shows very little change in the structure of the continuum emission as a function of wavelength (see also Fesen & Blair 1990). Hence, after subtracting sky background from each frame, an appropriate continuum frame can be aligned, scaled for relative throughput, and subtracted from an "emission line plus continuum" frame to obtain a nearly pure emission-line image. This also removes many of the stars in the emission line images to first order, although stellar residuals remain in some frames.

Figures 1*a*–1*d* show portions of several representative frames with the HUT aperture shown in projection. The astrometry involved measurement of star positions within the nebula relative to SAO stars (rms error = 1.″05) using special plates from the Harvard plate collection and a measuring engine at the Harvard-Smithsonian Center for Astrophysics. Since many of these secondary stars appear on the CCD frames, the center of the HUT aperture could be located with good accuracy. Inspection of video images of the acquisition field in the HUT TV guider has confirmed the aperture position relative to preplanned guide stars. The images shown in Figure 1 include lines of both medium and low ionization as well as a continuum band at 6100 Å. Some of the other frames listed in Table 2 differ from these in detail, but do not show additional bright filaments within the HUT aperture. This is important since some emission could have been missed because of finite filter widths in the Hα and [O III] images (see Table 2).

An examination of Figure 1*d* shows that the HUT aperture was filled with continuum emission, but that this emission was not uniformly distributed; the emission at the NE end of the slit (near the pulsar) was relatively bright. The emission-line gas appears to be largely dominated by a cluster of bright filaments near the center of the HUT aperture which are seen in both medium- and low-ionization images (e.g., [O III] and [O I], Figs. 1*b* and 1*c*). Other scattered filaments appear within the HUT aperture, but these are far less bright than the central filaments. These central filaments are the same filaments observed as *IUE*-P1 by Davidson et al. (1982) and will be discussed further below. While there may be differences between the distribution of a higher ionization line such as C IV and these lower ionization lines, the [O III] distribution does not look dramatically different from the other optical lines.

There are several stars within the projected HUT aperture. These stars are all fainter than the pulsar (marked with a "P" in Fig. 1), which has $V = 16.5$. However, if any one of these stars was particularly blue it might contaminate the HUT spectrum at a significant level. With two separate continuum frames (centered at 6100 and 8100 Å) we can investigate the approximate colors of these stars. We have performed a comparative analysis of these stars against the pulsar, which has $B - V = 0.5$ (Kristian 1971). All the stars in the HUT aperture have ratios of continuum count rates (6100/8100) very similar to the pulsar, indicating that they are also quite red. This is corroborated by UV images from the Ultraviolet Imaging Telescope on *Astro-1* (Hennessy et al. 1991, 1992). We conclude that no significant contamination of the UV continuum in the HUT spectrum is expected from these stars.

### 2.3. *Archival IUE Spectroscopy*

As part of a NASA Archival Data Program, we have reanalyzed the *IUE* data on the Crab Nebula, including the Position I and Position II data reported by Davidson et al. (1982), to search for spatial variations and to see whether other lines (or significant upper limits) might be present in these data. These data also have relevance to the interpretation of the HUT spectrum described above.

We obtained reprocessed line-by-line data files (sampled at 110 lines in the spatial direction, 30 lines of which correspond to the *IUE* large aperture) for all the relevant exposures and have reextracted the spectra, concentration on the short-wavelength (SWP) data. We have reduced the data using an IRAF[5]-based *IUE* reduction scheme developed at Johns

[5] IRAF is distributed by the National Optical Astronomy Observatories, which is operated by the Association of Universities for Research in Astronomy, Inc. (AURA), under cooperative agreement with the National Science Foundation.

Hopkins which yields results consistent with IDL-based reductions from the GSFC RDAF.

Because the individual exposures are quite long, there are typically a number of particle "hits" which need to be removed, as well as known "hot pixels" in the SWP camera (Bruegeman & Crenshaw 1989). After this "cleaning" procedure, the spatially resolved spectra can be converted into one-dimensional spectra representing either the whole *IUE* large aperture or various subsections of the large aperture as desired. Smoothed backgrounds, taken from regions adjoining the large aperture, were scaled, smoothed, and subtracted from these one-dimensional spectra before applying the *IUE* inverse sensitivity curves from Bohlin (1986).

Davidson et al. (1982) describe in detail the positioning (and uncertainty in positioning) of the separate exposures on the *IUE*-P1 region. Their "Figure 1" (slightly modified) is shown overlaid on the images in Figure 1 along with the HUT aperture. The majority of the total area covered by the various *IUE* aperture positions is within the HUT slit. The individual exposures are of some interest, but they are quite noisy. In Figure 3 we show our reextracted "average" *IUE*-P1 spectrum, obtained by summing all six long SWP spectra (31 hr of integration) and then rescaling the fluxes to an equivalent single *IUE* large aperture area. This figure has been smoothed with a three-point boxcar filter with the "splot" task in IRAF. Figure 3 can be compared directly with Figure 6 of Davidson et al. (1982). (Note that no shifting in wavelength space of the individual spectra has been attempted before adding, in contrast to Davidson et al. 1982.) Except for the improved spectral resolution gleaned from the reprocessing of the data, Figure 3 is quite similar to the results of Davidson et al. (1982); C IV, He II, and [C III] are the only lines clearly seen above the continuum. There are weak features at several wavelengths where lines might be expected (e.g., N V λ1240, C II λ1335, N III] λ1750, and others), but because of the quality of the data and the nature of the *IUE* detector, it is difficult to assess the reality of these features. In Table 1 we give measured fluxes and central wavelengths for the emission lines as well as upper limits for other features that may have significance in comparison with models. It is clear that the C IV and He II lines in the *IUE* data are blueshifted, but by a smaller amount than the blueshifted lines in the HUT data described above. *No redshifted components of these lines are seen associated with IUE-P1.* The position II spectrum, which was located near the pulsar and does include some filamentary emission (see Fig. 1*a*), shows only continuum emission in the SWP range.

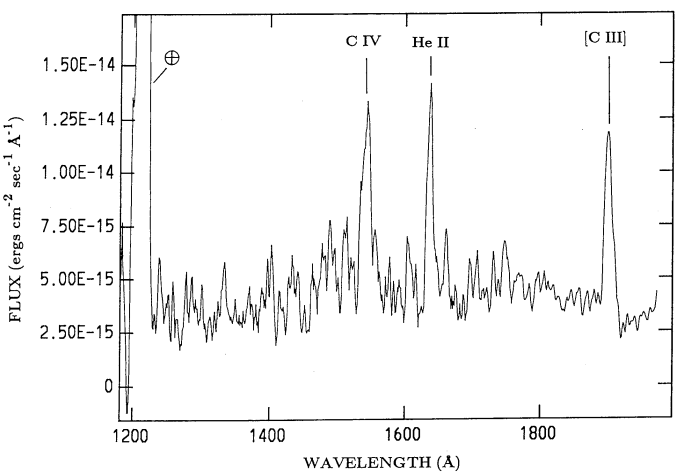


FIG. 3.—The total SWP *IUE* spectrum of the *IUE* Position I region after careful reprocessing from resampled *IUE* line-by-line data. The data were smoothed by a three-point boxcar filter (~3.5 Å). The fluxes have been scaled to an equivalent single *IUE* large aperture area. This spectrum represents 31 hr of total integration with *IUE*.

We have also used these data to investigate whether significant spatial variations in relative line intensities are present at *IUE*-P1. The total spatial extent covered by the long dimension of the *IUE* apertures (see Fig. 1) was divided into three equal sections, roughly corresponding to (A) the SW bright filament section (approximately half in and half out of the HUT aperture), (B) the bright filament cluster centrally located in the HUT aperture, and (C) the fainter, more flocculent emission filling the northwestern portion of the area observed by *IUE*. Assuming the nominal aperture positions shown by Davidson et al. (1982), lines from each SWP spectrum corresponding to each of these three spatial regions have been extracted. These separate subsections were then added to obtain representative spectra for the three spatial regions. The position A, B, and C spectra contain 38, 89, and 27 lines from the various line-by-line data files, respectively. The measured fluxes for these three extractions are also shown in Table 1.

There are no strong spatial effects in these spectra; some changes are seen in the relative intensities of the lines and in the faint features mentioned in the discussion above, but these can all be considered "in the noise." For instance, the measurements of the C IV:He II:[C III] ratios in the A, B, and C spectra are not always consistent with the *IUE*-P1 average spectrum of which they are a subset. This is a result of uncertainty in continuum placement and measurement of the noisy C IV line in these data (to which the other line intensities are referenced). The possible weak N V feature appears to be isolated in the region A spectrum, while the possible N III] λ1750 feature appears to be isolated in the region B spectrum. There is a camera feature near 1750 Å in the SWP camera, which makes the reality of the latter feature questionable. The weak features near C II λ1335 and O III] λ1663 appear marginally in all three subsections. The known camera hot pixels near 1663 Å were removed to first order in the reduction, although some residual effects from this cannot be ignored. There are no known camera features near 1240 Å or 1335 Å, but the purported lines at these wavelengths are very faint, and they are not blueshifted like the stronger lines are. We conclude that these features are also noise.

Ionization changes might be expected as a function of position if one region contains more low-density/high-ionization emission ("envelope" emission) while another position is dominated by higher density filament "cores." Toward this end, it is somewhat disappointing that N V or relatively strong C IV emission does not appear in the region C spectrum, since this region includes more flocculent, presumably lower density (higher ionization) material. Given that the signal-to-noise ratio of the data is low (and intrinsically difficult to quantify with *IUE*), it is difficult to claim that any of the observed changes are significant.

While the spatial changes in relative line intensities must be small, the absolute line fluxes are brightest in region C. (Note that the continuum fluxes in the A, B, and C spectra are essentially identical, as expected since the diffuse continuum is distributed throughout the region.) Hence, there is some evidence that the higher ionization UV lines are not distributed exactly like the optical emission, which is brightest in region B.

## 3. DISCUSSION

### 3.1. *Comparison of IUE and HUT Results*

The continuum flux observed by HUT very nearly scales to the *IUE* continuum flux by the ratio of the aperture areas. This is fortuitous since (assuming the UV continuum is distributed in a manner similar to the optical continuum) the continuum flux is not uniform within the HUT aperture. The position of the *IUE* filaments near the middle of the HUT aperture evidently approximates the "average" continuum level in the HUT aperture fairly well.

The measured emission-line wavelengths in the *IUE* data indicate the *IUE*-P1 filaments are blueshifted by $\sim 600$ km s$^{-1}$ with respect to rest wavelengths. This is somewhat less than the centroid of the blueshifted C IV and He II lines in the HUT spectrum. Ratios of the observed fluxes in these components between HUT and *IUE* are $\sim 2.7$ for C IV, and 2.1 for He II. Hence, $\sim 37\%$ of the blueshifted C IV observed by HUT can be attributed to *IUE*-P1, and $\sim 47\%$ of the He II. This indicates that the C IV:He II ratio in the remaining blueshifted emission in the HUT aperture (i.e. outside the *IUE*-P1 region) has a rather different value of $\sim 1.9$. This blueshifted emission may arise from a number of individually faint filaments or some more uniformly distributed component related to the approaching side of the shell.

The most startling difference between the HUT spectrum and the *IUE* data is the bifurcated C IV line. This component is present in various subsamples of the data and is not due to an instrumental artifact. The redshifted ($+1000$ km s$^{-1}$) component of C IV in the HUT data cannot be coming from the *IUE*-P1 filaments since it would have been readily detected even with *IUE*'s resolution of $\sim 10$ Å for extended sources. The filaments responsible for this emission are not readily apparent. While a number of other optical filaments are seen in projection within the HUT aperture, none approach the brightness of the *IUE*-P1 filaments. For instance, the filaments within the *IUE* position II aperture are some of the brighter filaments within the HUT aperture outside of the *IUE*-P1 region; however, these filaments are not responsible for the redshifted component in any significant way since the *IUE* position II data show only continuum emission. Whatever material is responsible for this redshifted emission has a ratio of C IV:He II $> 6$, based on the upper limit for redshifted He II from the HUT spectrum.

The power-law continuum from the diffuse synchrotron nebula within the HUT aperture extends to $\sim 1000$ Å in Figure 2, although the region between 1000–1150 Å shows considerable structure. Much of this structure can be attributed to molecular hydrogen absorption in the interstellar medium along the line of sight. In general, $E(B-V)$ and $N(H_2)$ show a good correlation above $E(B-V) = 0.1$ (Savage et al. 1977). Because of the low count rate in this region, we assume an $H_2$ column density scaled from the measured $E(B-V)$ rather than trying to fit $H_2$ absorption models to determine the column density. From Savage et al. (1977), we adopt $N(H_2) = 3 \times 10^{20}$ cm$^{-2}$. Using the $H_2$ model described by Bowers et al. (1992), we have calculated an $H_2$ attenuation profile for the region below 1150 Å; then, using various IRAF tasks, this model was appropriately scaled, smoothed, and divided into the Crab Nebula spectrum. The effect is relatively minor and raises the mean continuum level in the 1000–1150 Å range by $\sim 10\%$.

Finally, to minimize the effects of the Ly$\alpha$ and Ly$\beta$ geocoronal lines, we have used an appropriate portion of a pure nightglow spectrum taken with HUT using the same aperture during *Astro-1* and subtracted these regions from the Crab Nebula spectrum. The count rates in the HUT Crab Nebula data are in the regime of Poisson statistics; we have propagated the errors during the correction procedures discussed above.

We have fitted the continuum and lines in the corrected HUT spectrum using an IRAF task called "specfit," written by one of us (G. A. K.). This program reads in an array containing wavelengths, fluxes, and errors for each point and, employing user-specified inputs, fits the data by minimizing $\chi^2$ with a simplex search algorithm. Line and continuum components can both be fitted and the extinction correction can be fixed at a specified value or left as a free parameter. For continuum fitting we have binned the data by 6 pixels to increase the signal-to-noise ratio per bin and have chosen wavelength regions that avoid known emission lines and airglow features. For expressing the power-law exponent, $\alpha$, we adopt the convention where $I_\lambda \propto \lambda^{-\alpha}$. For comparison with *IUE* and other results, we have first fitted the region longward of 1230 Å and then included the region down to 1040 Å which is only available to HUT. Using the data longward of 1230 Å and leaving the extinction as a free parameter, we find $E(B-V) = 0.50^{+0.11}_{-0.06}$, $\alpha = 1.44^{+0.44}_{-0.26}$, and a reduced $\chi^2 = 1.17$ ($\chi^2 = 179$ for 156 data points and three degrees of freedom). The quoted errors correspond to 1 $\sigma$, and are quite large because the two free parameters are not independent (i.e., the contour in $\Delta\chi^2$ is an elongated ellipse; see Bevington 1969). The intrinsic flux predicted for 1000 Å from this model is $3.7 \times 10^{-12}$ ergs cm$^{-2}$ s$^{-1}$ Å$^{-1}$. This reddening value and slope of the power law are in good agreement with previous measurements. Wu (1981) found $E(B-V) = 0.50 \pm 0.03$ and $\alpha = 1.50$ (in our units) using broad-band photometric data for the inner 2.5 of the nebula from the *Astronomy Netherlands Satellite* (*ANS*).[6] Davidson et al. (1982) fitted both the SWP and LWR regions and used a $V$-band measurement to tie in with the optical region. Their dereddened continuum fit to *IUE* position II (near the pulsar) has an exponent of $\alpha = 1.5$ for an assumed reddening of $E(B-V) = 0.5$.

The *IUE*-P1 data ($\sim 1'$ SW of the pulsar) are consistent with a smaller exponent of $\alpha = 1.2$, although the error bars are large (see Fig. 8 of Davidson et al. 1982). This would seem to indicate a possible change in the power-law slope with radial position away from the pulsar. While such an effect is seen at larger radial distances in UV images from the Ultraviolet Imaging Telescope on *Astro-1* (Hennessy et al. 1991, 1992), the consistency between the *ANS* and HUT results argues against the reality of this change.

Including regions down to $\sim 1040$ Å (again excluding airglow lines) we have used "specfit" to find the following best fit to the continuum: $E(B-V) = 0.51^{+0.04}_{-0.03}$, $\alpha = 1.51^{+0.23}_{-0.23}$, and a reduced $\chi^2 = 1.14$ ($\chi^2 = 225.2$ for 200 data points and three degrees of freedom). The intrinsic flux at 1000 Å for this model is $4.2 \times 10^{-12}$ ergs cm$^{-2}$ s$^{-1}$ Å$^{-1}$. The reddening and exponent are similar to those found for the region above Ly$\alpha$, and

[6] Interestingly, one of the *ANS* passbands was centered at 1549 Å with a width of 149 Å, so one might expect some contamination from C IV $\lambda$1549. However, even over a relatively small bandpass such as this the continuum apparently dominates since the 1549 Å *ANS* point does not deviate from the power law. This is apparently corroborated by the UV imagery obtained by the Ultraviolet Imaging Telescope on *Astro-1*, which shows only continuum (i.e., no evidence of filaments) in an exposure centered near 1549 Å (Hennessy et al. 1991, 1992).

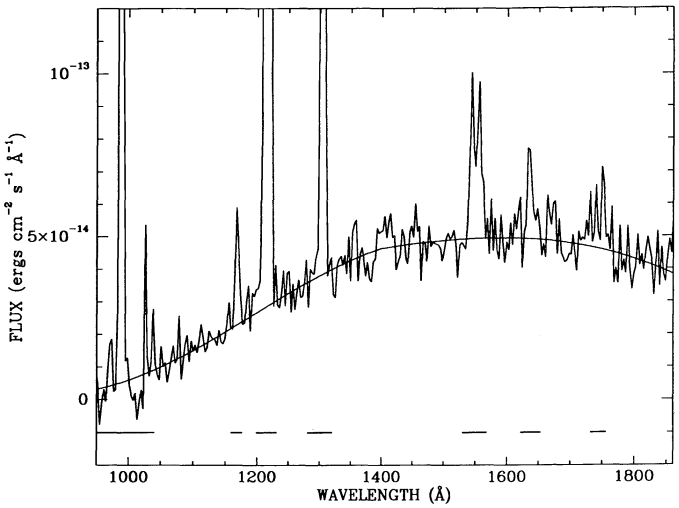


FIG. 4.—The best continuum fit to the HUT spectrum, using data binned over 6 pixels (~3 Å). Ly$\beta$ and the wings of the Ly$\alpha$ airglow lines were removed before binning. We find $\chi^2$ is minimized with $E(B-V) = 0.51$, $\alpha = 1.51$, and a reduced $\chi^2 = 1.14$ ($\chi^2 = 225.2$ for 200 data points and three degrees of freedom). As discussed in the text, we find no evidence for nonstandard extinction or any "turnover" in the power law over the HUT wavelength range. Note the marginal emission excesses near the expected positions of Si IV/O IV] $\lambda$1400, O III] $\lambda$1665, and N III] $\lambda$1750.

the reduced $\chi^2$ and 1 $\sigma$ errors are improved. This fit to the binned data is shown in Figure 4.

In frequency space, the X-ray power law has a steeper (i.e., more negative) slope than the optical/UV power law (see Davidson & Fesen 1985 and references therein). In wavelength units the optical/UV power-law exponent needs to decrease in order to connect with the X-ray power law. It is probable that the continuum shape at the shortest UV wavelengths shows no significant deviation from the power law at longer wavelengths, and that the turnover between the optical/UV power law and the X-ray power law occurs below ~1000 Å. Because of the reasonable fit obtained assuming the standard galactic extinction curve, we find no need to appeal to anomalous extinction in this direction. This is at odds with the conclusion of Wu (1981), who used the *ANS* data for stars in the direction of the Crab to infer that the UV extinction was peculiar.

The fit shown in Figure 4 was used with the unbinned HUT data to determine the emission-line strengths and upper limits on other lines that are shown in Table 1. From inspection of Figure 4, marginal excesses above the power law are seen at ~1745, 1660, and 1400 Å, roughly at the positions of N III], O III], and Si IV/O IV] emission lines. While these features are intriguing, they are only significant at the ~2 $\sigma$ level and cannot be considered clear "detections" of lines at these wavelengths.

### 3.2. *Optical Emission in the HUT and IUE Apertures*

To investigate the relative optical line strengths in the HUT and *IUE* apertures, we have measured the counts in boxes corresponding to the HUT and *IUE* apertures in our continuum-subtracted emission-line CCD images. The images were rotated by 45° to place the HUT aperture edges along lines and columns (only approximate for *IUE*-P1), and the IRAF task "imstat" was used to obtain the relative brightnesses in the *IUE*-P1 and HUT apertures. The results of this exercise are summarized in the last column of Table 2.

This comparison shows that in general ~35%–50% of the emission in strong optical lines can be attributed to *IUE*-P1, especially for those filters broad enough that they should not be missing any emission due to Doppler effects (e.g., [O I], He I, [C I]). As shown in Table 2, the [O III] filter is offset somewhat to redshifted velocities, and should not miss any redshifted emission; it could be missing some blueshifted emission, which dominates *IUE*-P1. It is interesting, however, that the derived ratio from our [O III] image is not substantially different from the He I result, for which a broader filter was used. The ratio of optical He I at the *IUE*-P1 and HUT positions is very similar to the ratio derived for He II $\lambda$1640 above from the *IUE*-P1 and HUT blueshifted data. It would be interesting to know whether the optical He I emission arises mainly in a blueshifted component like the He II does.

We have inspected Fabry-Perot data for the Crab Nebula in [O III] $\lambda$5007 kindly provided by A. Uomoto (see Uomoto et al. 1990). These data cover the velocity range $\pm$1800 km s$^{-1}$ in ~130 km s$^{-1}$ steps. In Figure 5 we show the summed intensities of the [O III] emission in the HUT and *IUE*-P1 apertures as a function of velocity from these data. The emission in the *IUE* region is dominated by a blueshifted component at about $-$600 km s$^{-1}$ with only a minor redshifted peak. The emission in the HUT aperture shows two broad peaks of comparable intensity (redshifted component ~$\frac{2}{3}$ the strength of the blueshifted component) centered at about $\pm$1100 km s$^{-1}$. These results are very consistent with the results of the UV spectra reported above (although the redshifted C IV component is somewhat *stronger* than the blueshifted component, in contrast to the optical [O III] result).

Interestingly, the brightest blueshifted [O III] filaments by a large factor are those near $-$600 km s$^{-1}$, corresponding to the bright filaments at *IUE*-P1. These filaments are considerably less blueshifted than the bulk of the material responsible for the blueshifted [O III] within the HUT aperture (and by analogy, the blueshifted C IV and He II lines in the HUT spectrum).

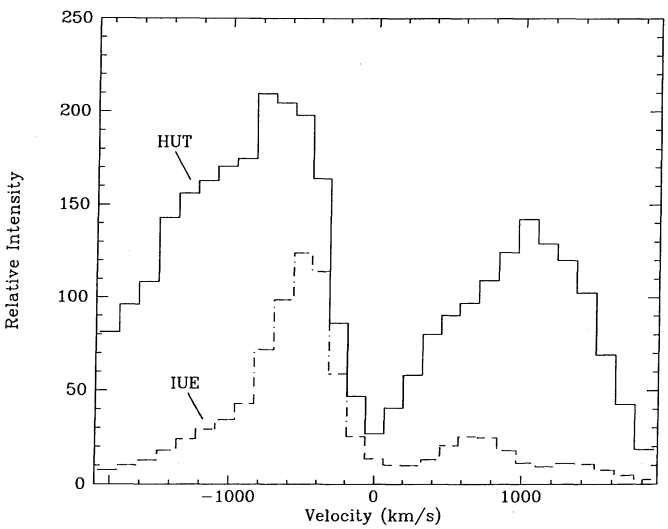


FIG. 5.—A summary of the optical [O III] $\lambda$5007 intensity as a function of velocity within the HUT and *IUE* position I apertures, from imaging Fabry-Perot data provided by A. Uomoto of Johns Hopkins. Note the much stronger double-peaked structure for the emission within the HUT aperture as compared with *IUE*. Also note that the blueshifted *IUE* emission is centered at lower velocities than the mean of the blueshifted emission in the HUT aperture, in accord with the UV spectral results.

Since the [O III] filamentary emission is fainter at larger blueshifts, the bulk of the emission must arise in a lower surface brightness, distributed component filling the aperture. Likewise at redshifted velocities, and in particular near $+1100 \pm 300$ km s$^{-1}$, no bright [O III] filaments are seen that might dominate the emission near this velocity and be responsible for the redshifted C IV. If the C IV and He II emission seen with HUT is associated with the [O III]–emitting material in the Fabry-Perot data, it seems likely that these emissions arise in optically faint filaments or a more diffuse component filling the HUT aperture. Additional UV data, especially with spatial resolution, could address this situation specifically.

### 3.3. *Comparison to Models*

With known large variations in the optical spectra of various filaments in the Crab Nebula (and without optical spectra that correspond exactly with the HUT aperture), we are limited in the extent to which comparisons with models can be made. However, the HUT data, in conjunction with those from *IUE*, make it clear that there are substantial variations in the He II:C IV ratio that have not been recognized previously. The *IUE*-P1 data have a He II:C IV ratio near unity. These data have been used with optical spectra to infer that the carbon abundance is roughly solar (Davidson et al. 1982). This in turn has been taken to represent the norm for the Crab and has been used to derive the probable mass range of the precursor star (Nomoto et al. 1982). However, we have now shown that the blueshifted data distributed throughout the HUT aperture (i.e., excluding the *IUE* filaments) has a He II:C IV ratio about half that of the *IUE* filaments, and the redshifted HUT component (also presumably distributed in a fairly diffuse component) has an even more extreme ratio of He II:C IV $\leq 0.15$. Since the ionization potentials for these two ions are quite different (24.6 eV to ionize $He^0$ to $He^+$, and 47.9 eV to ionize $C^{+2}$ to $C^{+3}$), we need to investigate in a general way whether these variations can be attributed to ionization effects or relative abundance variations.

Toward this end, we have calculated photoionization models using the program CLOUDY (Ferland 1990) version 80.07, the basic details of which are described by Baldwin et al. (1991). We adopted a plane-parallel geometry for the models, which should represent the observed structure of the filaments more closely than spherical geometry (Davidson 1973). The shape of the ionizing spectrum for these calculations was assumed to be that given by Davidson & Fesen (1985). In further describing the ionizing radiation, it is convenient to use the ionization parameter, $U$, which is essentially the ratio of ionizing photons to gas particles. In plane-parallel geometry $U = \phi/cN$, where $\phi$ is the total flux of photons with energies above the Lyman limit in units of photons cm$^{-2}$ s$^{-1}$ striking the gas and $N$ is the total gas density, which we took to be $10^3$ cm$^{-3}$ throughout the study. (This density is high enough to be a reasonable representation of densities in the filaments and low enough that collisional deexcitation should not affect the models.) To locate a starting point for our models, we adjusted the value of log $U$ until a calculated filament spectrum roughly matched the "average" UV/optical spectrum given in Davidson & Fesen (1985), assuming a composition with He at 4 times its solar abundance by number and all heavier elements at their solar values. The value of log $U$ determined in this way was $-2.25$, which is similar to values employed by Henry & MacAlpine (1982) in their photoionization models of Crab filaments. The solar abundances by mass fraction for several of the important elements in the models were taken from Anders & Grevesse (1989) and are He = 0.27, C = $3.06 \times 10^{-3}$, N = $1.11 \times 10^{-3}$, O = $9.63 \times 10^{-3}$, S = $4.17 \times 10^{-4}$, and Fe = $1.27 \times 10^{-3}$. Finally, we note that the models also take into account the effects of Bowen fluorescence on the He II line intensity (see Osterbrock 1989; Eastman et al. 1985).

We next calculated a set of models designed to test the effect of He abundance on the ratio of He II $\lambda$1640:C IV $\lambda$1549 by varying the mass fraction of He stepwise from its solar value up to 0.93 while holding log $U$ constant at $-2.25$ and maintaining the metal abundances at their solar mass fractions. Figure 6 shows the predicted He II:C IV line ratio as a function of relative He abundance, where the present model results are indicated with filled circles. Also shown at the right in Figure 6 are the blueshifted He II:C IV line ratios observed at *IUE*-P1 and by HUT, as well as the distributed HUT blueshifted component (HB$-$*IUE*). Likewise, the upper limit to the ratio observed by HUT for the redshifted material is indicated. The rapid rise in the line ratio with increasing He abundance is due to the relation between the actual number density (i.e., the number of emitters) and mass fraction of He. Notice that the models with log $U = -2.25$ all lie above the data in Figure 6, which could indicate that the value of log $U$ determined above is too low or that some other parameter is affecting the ratio as well (see below).

The top curve in Figure 6 indicates that differences in He abundance variations alone cannot explain the observed difference in line ratios between the blueshifted and redshifted material. Therefore, we have investigated ionization effects on the ratio by repeating the previous calculations with ionization parameters of log $U = -2.00$ and $-1.00$. These results are shown in Figure 6 with filled squares and filled triangles, respectively. The dramatic drop in the line ratio for these sets of models can be traced to changes in ionization structure of

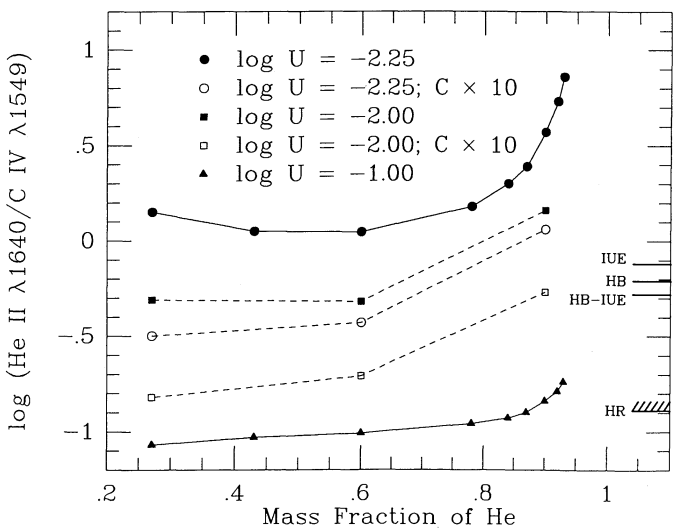


FIG. 6.—A summary of the predicted He II:C IV ratios as a function of He mass fraction for the models discussed in the text. The parameter $U$ describes the strength of the ionizing radiation. The tick marks at right indicate the observed ratios in the *IUE* position I data (*IUE*), the blueshifted HUT component (HB), the HUT blueshifted component after removal of the *IUE* emission (HB$-$*IUE*), and the HUT redshifted component (HR, upper limit only). Open symbol models have enhanced C abundances relative to the same shaped solid symbols. See text for specific model parameters.

oxygen when log $U$ is increased, resulting in much less $O^{+2}$ in the $C^{+3}$ zone. Much of the cooling in this case shifts to C IV $\lambda$1549, causing the He II $\lambda$1640:C IV $\lambda$1549 ratio to fall. Values of log $U$ between $-2.25$ and $-1.0$ can explain the observed UV line ratios with solar metal abundances and with solar or enhanced He abundances (although the highest He abundance log $U = -1.0$ models do not match the upper limit for the redshifted component).

The idea that a range of ionization parameters may be present within the HUT aperture is surely reasonable at some level; Fesen & Kirshner (1982) measured densities of individual filaments in the Crab to be in the range 550–3500 $cm^{-3}$, and material at such different densities will have different ionization parameters. However, the fact that there are few distinct filaments within the HUT aperture outside the *IUE*-P1 region argues for the presence of a diffuse component of emission. (The possible existence of low-density material in the Crab Nebula has been considered before, in particular by Davidson 1978). Since this diffuse component is not readily visible on optical images of the Crab, its emission measure is quite low, and thus it must be much lower density than the *IUE* filaments. This material would be represented by higher log $U$ values.

However, if the HUT blueshifted component (minus the *IUE* filaments) and the HUT redshifted component represent diffuse emission distributed throughout the aperture, one would not expect the ionization parameter of these components to be very different from one another. To account for the difference in He II:C IV ratio of these two components with ionization parameter alone would require a factor of 4 difference in the mean density of this diffuse component on the near and far sides of the expanding shell. Also, since the emissivity of this gas should scale as the density squared, one might expect an observable variation in the brightness of the diffuse gas from bright (on the near side) to faint (on the far side), which is not observed in the F-P data. Depending on the extent of He abundance variations in the observed material, it may be necessary to appeal to C abundance variations as well.

In order to test the effect of the C mass fraction on the line ratio, we have computed additional models at three different He mass fractions for log $U = -2.25$ and $-2.0$, but with the C mass fraction raised to a level 10 times its solar value. These results are indicated with open circles and open squares, respectively, in Figure 6. The increased C abundance lowers the predicted line ratio significantly in a manner that essentially parallels a changing ionization parameter. However, to account for the difference in observed ratio for the HUT blueshifted and redshifted components with a varying C abundance alone would require more than a factor of 10 in relative C abundance. Varying both He and C abundances might reduce the magnitude of the abundance variations needed to a more acceptable level. Also, clearly ionization and abundances could be changing between these components.

Circumstantial evidence for an elevated C abundance may come from the work of MacAlpine et al. (1989). These authors claimed that the high He torus (of which the *IUE* filaments are a part) was composed of 95% He by mass. Since these measurements pertain to the dense filaments, presumably a value of log $U$ near $-2.25$ is appropriate. However, at such extreme He abundance (far right in Fig. 6), the ratio predicted by the models is far above the observed ratio for *IUE* P1; an elevated C abundance could be used to match the model to the observed He II:C IV ratio. The high He abundance derived by MacAlpine et al. (1989) depends on the assumption that the optical He I lines are formed entirely by recombination, which may not be the case. If collisional processes affect the He I lines, it may be the derived He abundance that is in error.

While an enhanced C abundance cannot be claimed from the present data and modeling, neither can it be eliminated as a possibility. The *IUE* data from Davidson et al. (1982) and the claim that the C abundance in the Crab filaments is not enhanced has been used by Nomoto et al. (1982) to restrict the mass range of the precursor star of the Crab supernova. Our data show that the inference of roughly solar carbon abundance is not necessarily valid, and conclusions about the precursor mass based on the carbon abundance cannot be drawn. If the density and ionization of the diffuse component seen with HUT can be constrained with appropriate optical observations, it may be possible to address the question of the C abundance in the Crab Nebula in a meaningful way.

## 4. SUMMARY

We present ultraviolet spectroscopic data on the Crab Nebula obtained with the Hopkins Ultraviolet Telescope during the *Astro-1* space shuttle mission. We also present reprocessed *IUE* spectra for the Crab Nebula and compare these data to the HUT spectrum. The filaments observed with *IUE*, which are located near the center of the HUT aperture, produce blueshifted emission lines which are a subset of the blueshifted emission seen in the larger HUT aperture; the ratio of He II $\lambda$1640:C IV $\lambda$1549 varies by about a factor of 2 between the *IUE* and HUT blueshifted components. The HUT spectrum also shows a redshifted C IV line with no corresponding He II emission. Hence, we have demonstrated for the first time that significant relative UV line intensity variations exist in the Crab Nebula. We have calculated grids of plane-parallel photoionization models to investigate the parameters that may be responsible for these line intensity variations. The UV line ratios can be explained if a sufficiently large variation in ionization parameter is present in the material sampled with the HUT aperture. However, abundance variations are not ruled out as a contributing factor, and C abundances elevated by a factor of 10 or more above solar could be present. These results can be refined by incorporating appropriate optical data to further constrain the comparison with models.

We thank our colleagues on the HUT operations team and the Mission Operations Support group at the Marshall Space Flight Center for their support during the *Astro-1* Mission. We also thank the crew of the *Astro-1* mission for their successful efforts to overcome the problems encountered during the flight. Chris Arnade and David Handwerger assisted in the rereduction of the *IUE* spectra. Alan Uomoto shared the Fabry-Perot data with us, and Greg Hennessy informed us of the UIT results prior to publication, for which we are most grateful. The *IUE* work was supported by NASA grant NAG 5-988, and the Hopkins Ultraviolet Telescope project is supported by NASA contract NAS 5-27000 to the Johns Hopkins University.

## REFERENCES


Anders, E., & Grevesse, N. 1989, Geochim. Cosmochim. Acta, 5353, 197
Baldwin, J. A., Ferland, G. J., Martin, P. G., Corbin, M. R., & Cota, S. A. 1991, ApJ, 374, 580
Bevington, P. R. 1969, Data Reduction and Error Analysis for the Physical Sciences (New York: McGraw-Hill), 243
Blair, W. P., & Gull, T. R. 1990, S&T, 79, 591
Bohlin, R. C. 1986, ApJ, 301, 1001
Bowers, C. W., et al. 1992, ApJ, submitted
Bruegeman, O., & Crenshaw, D. M. 1989, *IUE* Newsletter, No. 37, 36
Davidsen, A. F., et al. 1992, ApJ, 392, 264
Davidson, K. 1973, ApJ, 186, 223
———. 1978, ApJ, 220, 177
———. 1979, ApJ, 228, 179
Davidson, K., & Fesen, R. A. 1985, ARAA, 23, 119
Davidson, K., Gull, T. R., Maran, S. P., Stecher, T. P., Fesen, R. A., Parise, R. A., Harvel, C. A., Kafatos, M., & Trimble, V. L. 1982, ApJ, 253, 696
Dennefeld, M., & Andrillat, Y. 1981, A&A, 103, 44
Eastman, R. G., MacAlpine, G. M., Kirshner, R. P., & Henry, R. B. C. 1985, in The Crab Nebula and Related Supernova Remnants, ed. M. C. Kafatos & R. B. C. Henry (Cambridge Univ. Press), 19
Ferland, G. J. 1990, Ohio State Univ. Internal Rep., No. 90-02
Fesen, R. A., Becker, R. H., & Goodrich, R. W. 1988, ApJ, 329, L89
Fesen, R. A., & Blair, W. P. 1990, ApJ, 351, L45
Fesen, R. A., & Kirshner, R. P. 1982, ApJ, 258, 1
Hennessy, G. S., O'Connell, R. W., Bohlin, R. C., Collins, N. R., Gull, T. R., Isensee, J. E., Landsman, W. B., Roberts, M. S., Smith, A. M., & Stecher, T. P. 1992, ApJ, 395, L13
Hennessy, G. S., O'Connell, R. W., Collins, N., Gull, T. R., Isensee, J., Landsman, W. B., & Stecher, T. P. 1991, BAAS, 23, 916
Henry, R. B. C. 1986, PASP, 98, 1044
Henry, R. B. C., & MacAlpine, G. M. 1982, ApJ, 258, 11
Hester, J. J., Graham, J. R., Beichman, C. A., & Gautier, T. A. 1990, ApJ, 357, 539
Kafatos, M. C., & Henry, R. B. C., ed. 1985, The Crab Nebula and Related Supernova Remnants, (Cambridge Univ. Press)
Kristian, J. 1971, in IAU Symp. 46, The Crab Nebula, ed. R. D. Davies & F. G. Smith (Dordrecht: Reidel), 87
Longo, R., Stalio, R., Polidan, R. S., & Rossi, L. 1989, ApJ, 339, 478
MacAlpine, G. M., McGaugh, S. S., Mazzarella, J. M., & Uomoto, A. 1989, ApJ, 342, 364
MacAlpine, G. M., & Uomoto, A. 1991, AJ, 102, 218
Mathis, J. S. 1990, ARAA, 28, 37
Miller, J. S. 1973, ApJ, 180, L83
———. 1978, ApJ, 220, 490
Nomoto, K. 1984, ApJ, 277, 791
Nomoto, K., Sparks, W. M., Fesen, R. A., Gull, T. R., Miyaji, S., & Sugimoto, D. 1982, Nature, 299, 803
Osterbrock, D. E. 1989, Astrophysics of Gaseous Nebulae and Active Galactic Nuclei (Mill Valley, CA: University Science Books)
Pequignot, D., & Dennefeld, M. 1983, A&A, 120, 249
Savage, B. D., Bohlin, R. C., Drake, J. G., & Budich, W. 1977, ApJ, 216, 291
Seaton, M. J. 1979, MNRAS, 187, 73P
Smith, R. C., Kirshner, R. P., Blair, W. P., & Winkler, P. F. 1991, ApJ, 375, 652
Uomoto, A., & MacAlpine, G. M. 1987, AJ, 93, 1511
Uomoto, A., MacAlpine, G., Woodgate, B., Lowenthal, J., Brown, L., & Oliversen, R. 1990, BAAS, 22, 751
Weidemann, V., & Koester, D. 1983, A&A, 121, 77
Woosley, S. E., & Weaver, T. A. 1982, in Supernovae: A Survey of Current Research, ed. M. J. Rees & R. J. Stoneham (Dordrecht: Reidel), 79
Wu, C.-C. 1981, ApJ, 245, 581